Constraints on the Dark Matter Particle Mass from the Number of Milky Way Satellites

Emil Polisensky[1,2] and Massimo Ricotti[2]

[1] *Naval Research Laboratory*
[2] *University of Maryland*[*]

(Dated: April 12, 2010)

We have conducted N-body simulations of the growth of Milky Way-sized halos in cold and warm dark matter cosmologies. The number of dark matter satellites in our simulated Milky Ways decreases with decreasing mass of the dark matter particle. Assuming that the number of dark matter satellites exceeds or equals the number of observed satellites of the Milky Way we derive lower limits on the dark matter particle mass. We find with 95% confidence $m_s > 11.8$ keV for a sterile neutrino produced by the Dodelson & Widrow mechanism and $m_{WDM} > 2.1$ keV for a thermal dark matter particle. The recent discovery of many new dark matter dominated satellites of the Milky Way in the Sloan Digital Sky Survey allows us to set lower limits comparable to constraints from the complementary methods of Lyman-α forest modeling and the unresolved cosmic X-ray background. Future surveys like LSST, DES, PanSTARRS, and SkyMapper have the potential to discover many more satellites and further improve constraints on the dark matter particle mass.

I. INTRODUCTION

Cold dark matter (CDM) is extremely successful at describing the large scale features of matter distribution in the Universe but has problems on small scales. Below the Mpc scale CDM predicts numbers of satellite galaxies for Milky Way-sized halos about an order of magnitude in excess of the number observed. This is the 'missing satellites' problem [1, 2]. One proposed solution is that, due to feedback mechanisms, dark matter satellites below a certain scale do not form stars and are nonluminous dark halos. Another solution is the dark matter may be 'warm' (particle mass ~ 1 keV) instead of 'cold' (particle mass ~ 1 GeV). By reducing the dark matter particle mass, streaming motions can erase density fluctuations on small scales and reduce the number of satellites. Warm dark matter (WDM) models have been studied through N-body simulations by a number of authors [3–8].

A complication arises when running N-body simulations of WDM cosmologies due to numerical artifacts produced by discrete sampling of the gravitational potential with a finite number of particles. That discreteness effects are a problem for simulations started from lattice-like initial conditions has long been known (see [9] for a review). Particles are positioned on a regular, uniform lattice and then their positions are perturbed by a random realization of the linear fluctuation field associated with the choice of cosmology. Perturbations collapse and form filaments with nonphysical clumps separated by a distance equal to the lattice spacing (see Figure 1). Wang & White [10] have shown that discreteness also affects simulations started from glass-like conditions. A glass is created by advancing a random distribution of particles under repulsive gravitational forces until the system reaches quasi-equilibrium and the total force on each particle vanishes. The particle positions are then perturbed from this state as for the lattice. Wang & White showed that even under these conditions, with no large-scale order, filaments still fragment into halos with separation equal to the mean particle separation in the glass. These halos are nonphysical numerical artifacts. The ability of these halos to survive disruption as they accrete from filaments onto a Milky Way-sized halo has not been studied, but they may contaminate the satellite distribution in WDM simulations.

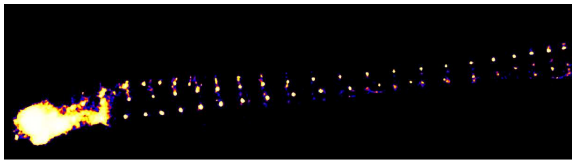

FIG. 1. "Poisson noise" halos formed along a filament and accreting onto a larger halo at $z = 1$ in a WDM simulation ($m_{WDM} = 1$ keV). These halos are numerical artifacts.

In the last few years 16 new dwarf spheroidal galaxies have been discovered in the Sloan Digital Sky Survey (SDSS) [11] (see Table 3 and references therein). After correcting for completeness the estimated number of Milky Way satellites is > 60. These new dwarfs have low luminosities, low surface brightnesses, and are dark matter dominated. Since the number of dark matter halos must be greater than or equal to the number of observed satellites, the new data from the SDSS may provide interesting limits on how cold the dark matter is.

Motivated by the recent increase in the number of observed Milky Way satellites and by the need to better understand discreteness effects, we have performed new simulations of the growth of a Milky Way-like galaxy in CDM and WDM cosmologies for a variety of WDM particle masses. Our goal is to constrain the dark matter particle mass by comparing the number of satellite ha-

[*] emilp@astro.umd.edu

Report Documentation Page

Form Approved
OMB No. 0704-0188

1. REPORT DATE	2. REPORT TYPE	3. DATES COVERED
12 APR 2010		**00-00-2010 to 00-00-2010**

4. TITLE AND SUBTITLE	5a. CONTRACT NUMBER
Constraints on the Dark Matter Particle Mass from the Number of Milky Way Satellites	5b. GRANT NUMBER
	5c. PROGRAM ELEMENT NUMBER
6. AUTHOR(S)	5d. PROJECT NUMBER
	5e. TASK NUMBER
	5f. WORK UNIT NUMBER
7. PERFORMING ORGANIZATION NAME(S) AND ADDRESS(ES) **Naval Research Laboratory,Adelphi,MD,20783**	8. PERFORMING ORGANIZATION REPORT NUMBER
9. SPONSORING/MONITORING AGENCY NAME(S) AND ADDRESS(ES)	10. SPONSOR/MONITOR'S ACRONYM(S)
	11. SPONSOR/MONITOR'S REPORT NUMBER(S)

12. DISTRIBUTION/AVAILABILITY STATEMENT
Approved for public release; distribution unlimited

13. SUPPLEMENTARY NOTES

14. ABSTRACT

15. SUBJECT TERMS

16. SECURITY CLASSIFICATION OF:			17. LIMITATION OF ABSTRACT	18. NUMBER OF PAGES	19a. NAME OF RESPONSIBLE PERSON
a. REPORT	b. ABSTRACT	c. THIS PAGE			
unclassified	**unclassified**	**unclassified**	**Same as Report (SAR)**	**15**	

los in the simulated Milky Way to the observed number of luminous satellites for the actual Milky Way. Macciò & Fontanot [8] combined N-body simulations with semi-analytic models of galaxy formation to compare the simulated and observed Milky Way satellite luminosity functions for CDM and WDM cosmologies. In this work, we do not make any assumptions on how we populate dark matter halos with luminous galaxies. We simply impose that the number of observed satellites is less than or equal to the number of dark matter halos for a range of Galactocentric radii. This guarantees a robust lower limit on the dark matter particle mass.

II. SIMULATIONS

All our simulations were conducted with the N-body cosmological simulation code GADGET-2 [12] assuming dark matter only simulations (we do not include the effect of baryons in our simulations). We adopted values for cosmological parameters from the third year release of the WMAP mission [13], (Ω_m, Ω_Λ, h, σ_8, n_s) = (0.238, 0.762, 0.73, 0.751, 0.951). For each simulation set we produced a single realization of the density field in the same periodic, comoving volume but varied the power spectrum of fluctuations appropriate for CDM and WDM cosmologies. Our initial conditions were generated on a cubic lattice using the GRAFIC2 software package [14]. The power spectra for CDM and WDM are given by

$$P_{CDM}(k) \propto k^{n_s} T^2_{CDM}, \quad (1)$$
$$P_{WDM}(k) = P_{CDM} T^2_{WDM}, \quad (2)$$

respectively, with the normalization of P_{CDM} determined by σ_8. We used the transfer function for CDM adiabatic fluctuations given by Bardeen et al. (BBKS) [15]:

$$T_{CDM}(k) = \frac{\ln(1+2.34q)}{2.34q} \left[1+3.89q+(16.1q)^2+(5.46q)^3+(6.71q)^4\right]^{-0.25} \quad (3)$$

where $q = k/(\Omega_m h^2)$. A potential problem with the BBKS transfer function is that it underestimates power on large scales. In the Appendix we investigate the effect that our choice for the CDM transfer function may have on the number of Milky Way satellites. We run one of our simulations adopting the transfer functions from Eisenstein & Hu [16] and we find that this does not affect our results on the number of satellites.

Assuming the WDM to be a thermal particle, a particle that was in thermal equilibrium with the other particle species at the time of its decoupling, we used the transfer function valid for thermal particles given by Bode, Ostriker, & Turok [5]:

$$T_{WDM}(k) = \left[1+(\alpha k/h)^\nu\right]^{-\mu}, \quad (4)$$

where $\nu = 2.4$, $\mu = 4.167$ and

$$\alpha = 0.0516 \left(\frac{m_{WDM}}{1\ \mathrm{keV}}\right)^{-1.15} \left(\frac{\Omega_m}{0.238}\right)^{0.15} \left(\frac{h}{0.73}\right)^{1.3} \left(\frac{g_X}{1.5}\right)^{-0.29}. \quad (5)$$

The parameter g_X is the number of degrees of freedom for the WDM particle, conventionally set to the value for a light neutrino species: $g_X = 1.5$. The parameter k is the spatial wavenumber in Mpc^{-1} and m_{WDM} is the mass of the WDM particle in keV.

A candidate for a thermal WDM particle is the gravitino, the superpartner of the graviton in supersymmetry theories. The lightest stable particle (LSP) in supersymmetry theories are natural dark matter candidates. If the scale where supersymmetry is spontaneously broken is $\lesssim 10^6$ GeV, as predicted by theories where supersymmetry breaking is mediated by gauge interactions, then the gravitino is likely to be the lightest stable particle and can have a mass reaching into the keV regime.

In general the dark matter particle may not have been in thermal equilibrium when it decoupled. This is the case for a sterile neutrino (see [17] and references therein), a theoretical particle added to standard electroweak theory, the only matter it interacts with (except through gravity) are left-handed neutrinos. There are several mechanisms by which sterile neutrinos can be produced . In the standard mechanism proposed by Dodelson & Widrow (DW) [18], sterile neutrinos are produced when oscillations convert some of the more familiar active neutrinos into the sterile variety. The amount produced depends on the sterile neutrino mass and the mixing angle but we will not consider such details here and when considering sterile neutrinos we simply assume they compose the entirety of the dark matter. The transfer function for DW sterile neutrinos with mass m_s is given by [19]:

$$T_s(k) = \left[1+(\alpha k/h)^\nu\right]^{-\mu}, \quad (6)$$

where $\nu = 2.25$, $\mu = 3.08$ and

$$\alpha = 0.1959 \left(\frac{m_s}{1\ \mathrm{keV}}\right)^{-0.858} \left(\frac{\Omega_m}{0.238}\right)^{-0.136} \left(\frac{h}{0.73}\right)^{0.692}. \quad (7)$$

Viel et al. [20] give a scaling relationship between the mass of a thermal particle and the mass of the DW sterile neutrino for which the transfer functions are nearly identical:

$$m_s = 4.379\ \mathrm{keV} \left(\frac{m_{WDM}}{1\ \mathrm{keV}}\right)^{4/3} \left(\frac{\Omega_m}{0.238}\right)^{-1/3} \left(\frac{h}{0.73}\right)^{-2/3}. \quad (8)$$

Other sterile neutrino production mechanisms include that of Shi & Fuller (SF) [21] who showed the DW mechanism is altered in the presence of a universal lepton asymmetry where production can be enhanced by resonance effects. Sterile neutrinos can also be produced from decays of gauge-singlet Higgs bosons at the electroweak scale [22]. The momentum distribution of the

sterile neutrinos depends on the production mechanism. In the absence of transfer function calculations we use the expressions in [17] for the free streaming length and average momentum to derive approximate scaling factors for the SF and Higgs produced sterile neutrinos: $m_{DW}/m_{SF} = 1.5$, $m_{DW}/m_{Higgs} = 4.5$.

There are ways other than warm dark matter to reduce small scale power. Broken-scale invariance inflation models [23] have a cutoff length below which power is suppressed. Particle theories where the LSP dark matter particle arises from the decay of the next lightest supersymmetric particle (NLSP) can also suppress small scale power if the NLSP is charged and coupled to the photon-baryon plasma [24] or if the NLSP decay imparts a large velocity to the LSP [25]. Our method can be applied to constrain these models as well. However, in the rest of this paper we will not discuss further the consequences that our work has on these theories.

In our simulations we assume the dark matter is thermal and scale the results to the standard sterile neutrino mass using Eq. (8). Our initial conditions include particle velocities due to the gravitational potential using the Zeldovich approximation but we do *not* add random thermal velocities appropriate for WDM to the simulation particles. Bode, Ostriker, & Turok [5] argue that for warm particle masses greater than 1 keV thermal motions are unimportant for halos on scales of a kiloparsec and above. Regardless, we expect thermal motions, if anything, would reduce the number of small mass halos and by not including thermal motions the mass limits derived from our simulations will be more conservative.

We ran simulations for CDM and WDM cosmologies with WDM particle masses of $m_{WDM} = 1$, 2, 3, 4, and 5 keV ($m_s = 4.4$, 11.0, 18.9, 27.8, 37.4 keV). Figure 2 shows the power spectra for these cosmologies along with the spectrum for an 11 keV standard sterile neutrino using Eq. (8). We ran two separate sets of simulations both consisting of a comoving cubic box 90 Mpc on a side. *Set A* consisted of 204^3 particles giving a 'coarse' particle mass of 3.0×10^9 $M_\odot$ and a force resolution of 8.8 kpc (all our force resolutions were fixed in comoving coordinates). We ran the HOP halo finding software [26] at $z = 0$ and identified Milky Way-sized halos with masses $1 - 2 \times 10^{12}$ $M_\odot$. Halos were examined visually, one was chosen that was at least several Mpc away from clusters and other large structures so as to be relatively isolated. Its particles were identified in the initial conditions and a cubic refinement level, 6.2 Mpc on a side, was placed on the region. For the refinement region in our low resolution simulations we used $11,239,424$ (224^3) particles with mass and force resolutions of 7.3×10^5 $M_\odot$ and 550 pc, respectively. For CDM and WDM particle masses of 1, 2, and 4 keV we also conducted higher resolution simulations with $89,915,392$ (448^3) particles in the refinement region and mass and force resolutions of 9.2×10^4 $M_\odot$ and 275 pc, respectively. The simulated Milky Way halo had a neighbor halo with mass $0.23 M_{MW}$ at a distance of 700 kpc in the low resolution simulations. The real Milky Way has a massive neighbor in M31, the Andromeda galaxy ($M_{And} \sim 1 - 3 M_{MW}$), at a distance $\sim$ 700 kpc. But in the higher resolution simulation this satellite is merging with the Milky Way at $z = 0$. Such a merger may disrupt the equilibrium of the halo and makes it nonrepresentative of the actual Milky Way. The difference between the high and the low resolution simulations is significant and complicates the comparison between the simulations.

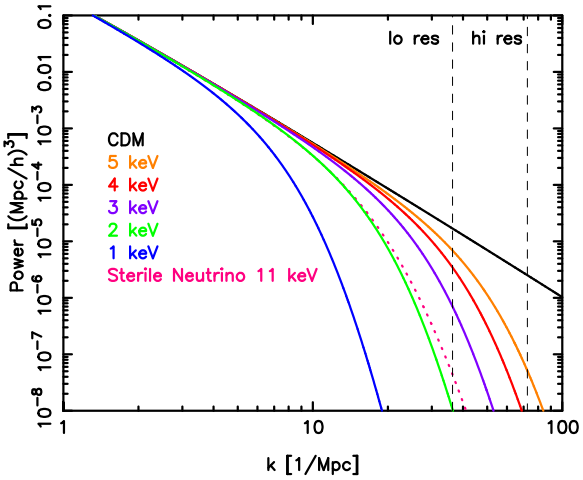

FIG. 2. Power spectra for our simulations. The dotted line is the power spectrum for an 11 keV standard sterile neutrino from Abazajian [19]. The neutrino spectrum is approximately the same as a 2 keV thermal particle, validating the scaling relation of Viel et al. [20]. The vertical dashed lines indicate the lattice cell size in our high and low resolution refinement levels.

The need to explore the scatter between the satellite distribution of different realizations of Milky Way-type halos, in addition to the complications arising with the high and low resolution simulations of *set A*, prompted us to conduct a new set of simulations. *Set B* consisted of 408^3 particles giving a coarse particle mass of 3.8×10^8 $M_\odot$ and a force resolution of 4.4 kpc. We ran HOP and identified halos with masses $0.8 - 2.2 \times 10^{12}$ $M_\odot$. For each halo we also found the nearest neighboring halo with mass $> 0.8 \times 10^{12}$ $M_\odot$. We selected a halo whose nearest massive neighbor was at least 5 Mpc away and visually verified the halo was indeed isolated. A rectangular refinement level $6.1 \times 7.0 \times 7.9$ Mpc was placed over this halo's particles in the initial conditions. Low and high resolutions were conducted with the same mass and force resolutions as *set A*. The low resolution simulations used $16,515,072$ ($\sim 255^3$) particles in the refinement level while high resolution used $132,120,576$ ($\sim 510^3$) particles in the refinement level.

Table I summarizes the properties of our simulated Milky Way halos at $z = 0$ in all the simulations. We write R_Δ to mean the radius enclosing an overdensity Δ times the critical value. The mass and number of particles inside R_Δ are M_Δ and N_Δ, respectively; v_Δ is the circular velocity $v_\Delta^2 \equiv GM_\Delta/R_\Delta$ at R_Δ, and v_{max} is the

maximum circular velocity of the halo.

Figure 3 shows the density profiles of the *A* and *B* Milky Way halos calculated by breaking the halo into spherical shells. Small differences between the high and low resolution *set A* halos caused by the merging neighbor are apparent but generally the profiles are very similar across all simulations of each set. We do not see an inner flattening of the halos in the WDM simulations because we did not add thermal motions to our particles. Figure 4 shows portraits of the Milky Way in our *set B* low resolution simulations.

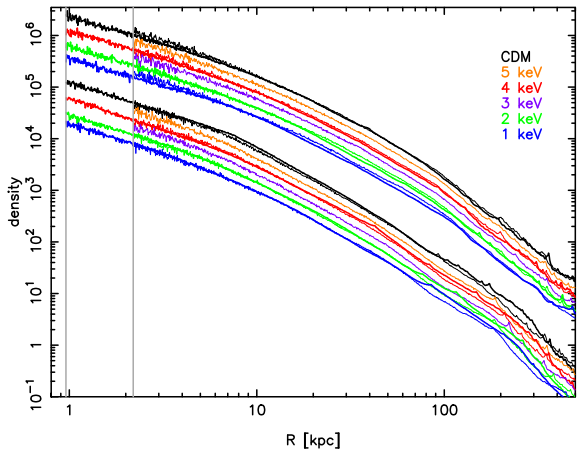

FIG. 3. Density profile of Milky Way halo in all simulations. Thick lines are the high resolution simulations. The *set A* simulations and the WDM cosmologies in each set have been offset downward for clarity. The profiles are plotted starting from the convergence radius of Power et al. [27] for both resolutions (vertical lines).

A. Identification of Satellites

Finding gravitationally bound dark matter halos in N-body simulations is accomplished with halo finding software employing a variety of algorithms. Traditional halo finders like FOF, DENMAX and its relatives HOP and SKID [26, 28–30], have difficulty finding satellite halos within a much larger host halo. New satellite-savvy halo finders such as 6DFOF, AHF, and SUBFIND [31–34], have been developed but require greater computational resources and are not always publicly available. Our approach is to first subtract the average density profile of the Milky Way from the particle densities, remove low density particles from the list, then run a traditional halo finder on the satellite cores that remain.

We calculated initial particle densities using the HOP software package smoothing over the 10 nearest neighbors. We broke the Milky Way halo into concentric shells with equal thickness in logarithmic radius from 0.1 to 500 kpc. In order to account for the triaxiality of halos, the shells were divided into 8 equal volume regions and the density in each was calculated. We subtracted these densities from the HOP particle densities. The number of shells was adjusted until good subtraction of the Milky Way profile was achieved, see Figure 5. We also tried ellipsoidal shells aligned with the axes of the halo but the improvement was negligible. Particles with low densities were removed and we ran SKID on the remaining particles with a linking length of 2 kpc and smoothing over 32 neighbors. Unbound particles were iteratively removed and we selected gravitationally bound halos with 10 or more particles.

SKID calculates properties of the halos it finds such as the total mass and the maximum circular velocity. For our purposes the maximum circular velocity is a better characteristic of a satellite than the mass because quantifying the outer boundary of a satellite embedded in a larger halo is complicated. Our subtraction of the Milky Way profile to isolate the satellites may also affect their outer boundaries. The max circular velocity however typically occurs at a radius well inside the satellite outskirts.

III. RESULTS

A. Satellite Distribution Functions

Figure 6 shows the cumulative max circular velocity function, $N(> v_{max})$, for all satellites within R_{50} of each simulated Milky Way. Also plotted are the fitting functions of $N(> v_{max})$ from the Via Lactea I and II and Aquarius simulations [32, 35, 36]. The target of these simulations were Milky Way sized halos with higher mass resolution than our simulation but for a CDM cosmology only. There is a large variation in magnitude between the simulations that cannot be explained as a resolution artifact or by differences in the adopted cosmological parameters. Diemand et al. [35] argued the difference between Via Lactea I and II lies within the halo-to-halo varance. The Aquarius simulation suite included 6 unique halos with a *rms* scatter of only 10% about the mean. The abundance of satellites in Via Lactea I is 69% lower than the Aquarius mean and Via Lactea II is 31% lower which led Springel et al. [36] to argue that the difference between Aquarius and Via Lactea is due to a systematic error in the Via Lactea realization of the initial conditions. Our CDM simulations have satellite abundances between Via Lactea I & II. Both Via Lactea and our simulations used initial conditions generated with GRAFIC2 which may be why our results disagree with Aquarius.

On the other hand, Ishiyama et al. [37] examined the satellite abundances of 68 simulated Milky Way sized halos. They claim their simulations agree with both Via Lactea and Aquarius. They also found a correlation between satellite abundance and halo concentration and between the maximum value of the radius enclosing half of the final virial mass. This suggests the number of satellites is determined by the formation epoch of the halo and at least partly by the assembly history of the halo. It is possible the small scatter in the Aquarius

TABLE I. Properties of simulated Milky Way halos.

Simulation	M_{200} $[10^{12}M_\odot]$	R_{200} [kpc]	M_{50} $[10^{12}M_\odot]$	R_{50} [kpc]	v_{50} [km/s]	v_{max} [km/s]	N_{200}	N_{50}
Set A								
CDM lo	1.2919	218.49	1.6792	378.49	138.14	183.34	1,760,904	2,288,747
5 keV lo	1.2991	218.90	1.6829	378.77	138.24	184.01	1,770,649	2,293,847
4 keV lo	1.2937	218.63	1.6838	378.90	138.25	184.62	1,763,346	2,295,103
3 keV lo	1.2882	218.36	1.6855	379.04	138.29	184.21	1,755,895	2,297,320
2 keV lo	1.3115	219.59	1.6703	377.81	137.89	182.55	1,787,535	2,276,577
1 keV lo	1.3056	219.32	1.6616	377.26	137.64	180.94	1,779,518	2,264,844
CDM hi	1.5278	231.10	2.0354	403.56	147.28	192.27	16,659,568	22,194,175
4 keV hi	1.5168	230.55	2.0403	403.97	147.39	190.74	16,538,776	22,247,815
2 keV hi	1.5272	231.10	2.0299	403.29	147.14	184.35	16,652,697	22,134,513
1 keV hi	1.5493	232.19	2.0254	402.88	147.05	179.96	16,893,692	22,084,649
Set B								
CDM lo	1.6440	236.85	2.1324	409.86	149.59	196.54	2,240,809	2,906,506
5 keV lo	1.6424	236.71	2.1255	409.45	149.42	196.49	2,238,592	2,897,056
4 keV lo	1.6417	236.71	2.1213	409.18	149.33	196.82	2,237,605	2,891,353
3 keV lo	1.6358	236.44	2.1186	409.04	149.25	196.40	2,229,660	2,887,665
2 keV lo	1.6128	235.34	2.0935	407.40	148.67	196.15	2,198,289	2,853,496
1 keV lo	1.5798	233.70	2.0750	406.16	148.23	193.26	2,153,349	2,828,261
CDM hi	1.5155	230.41	1.9966	400.96	146.35	194.99	16,525,148	21,771,052
4 keV hi	1.4883	229.04	1.9819	400.00	145.98	189.56	16,228,561	21,611,248
2 keV hi	1.4759	228.49	1.9667	399.04	145.59	186.01	16,093,504	21,444,730
1 keV hi	1.3843	223.56	1.8656	392.05	143.06	180.09	15,094,535	20,342,179

halos may be a selection effect. The 6 Aquarius halos were chosen because they hosted normal spiral galaxies in semi-analytic modeling and had no massive neighbors at $z = 0$, suggesting the halos had similar formation epochs and accretion histories. Ishiyama's halos were not selected by environment or accretion history. Indeed, their halos with the highest abundance of satellites have late formation epochs and are still undergoing major mergers, but such halos are unlikely to be representative of the Milky Way. Satellite mergers heat and potentially destroy the disks of spiral galaxies [38, 39]. The thick disk of the Milky Way is thought to have been created by a merger event about 12 billion years ago. The $10 - 12$ billion year old thin disk indicates the Milky Way has not suffered a major merger since $z \sim 1$. Aquarius' semi-analytic modeling shows their halos host Milky Way-type spiral galaxies and should be characteristic of the Milky Way. The Aquarius simulations also have the highest abundances of simulations attempting to represent the Milky Way. If the Aquarius results are correct and their satellite abundances represent the Milky Way, our simulations can be brought into agreement by multiplying the *set A* abundances by 2.5 and *set B* by 2.0.

B. Poisson Halos

We discussed in Section I that the discrete sampling of the matter density field in N-body simulations introduces Poisson noise to the power spectrum of density perturbations. The Poisson noise results in the formation of artificial small mass halos in WDM cosmologies. Plotted in Figure 7 are the circular velocity functions compared to analytical predictions using Press-Schechter theory [40]. Barkana, Haiman, & Ostriker [41] showed the effects of WDM on Press Schechter theory. We extend their work by also including the Poisson noise from the discreteness of the simulations. Our model of the effect of Poisson noise on the power spectrum is analogous to the one in Afshordi, McDonald, & Spergel [42], that considered the case of dark matter composed of primordial black holes. They showed that the fluctuation in the number of primordial black holes due to Poisson noise leads to the addition of a constant term to the linear power spectrum that becomes dominant at small scales. We add a constant Poisson noise term to the power spectrum in our Press-Schechter calculations. The addition of Poisson noise produces the upturns at low velocities in Figure 7. These upturns are also apparent in the simulations of Bode, Ostriker, & Turok [5] and Barkana, Haiman, &

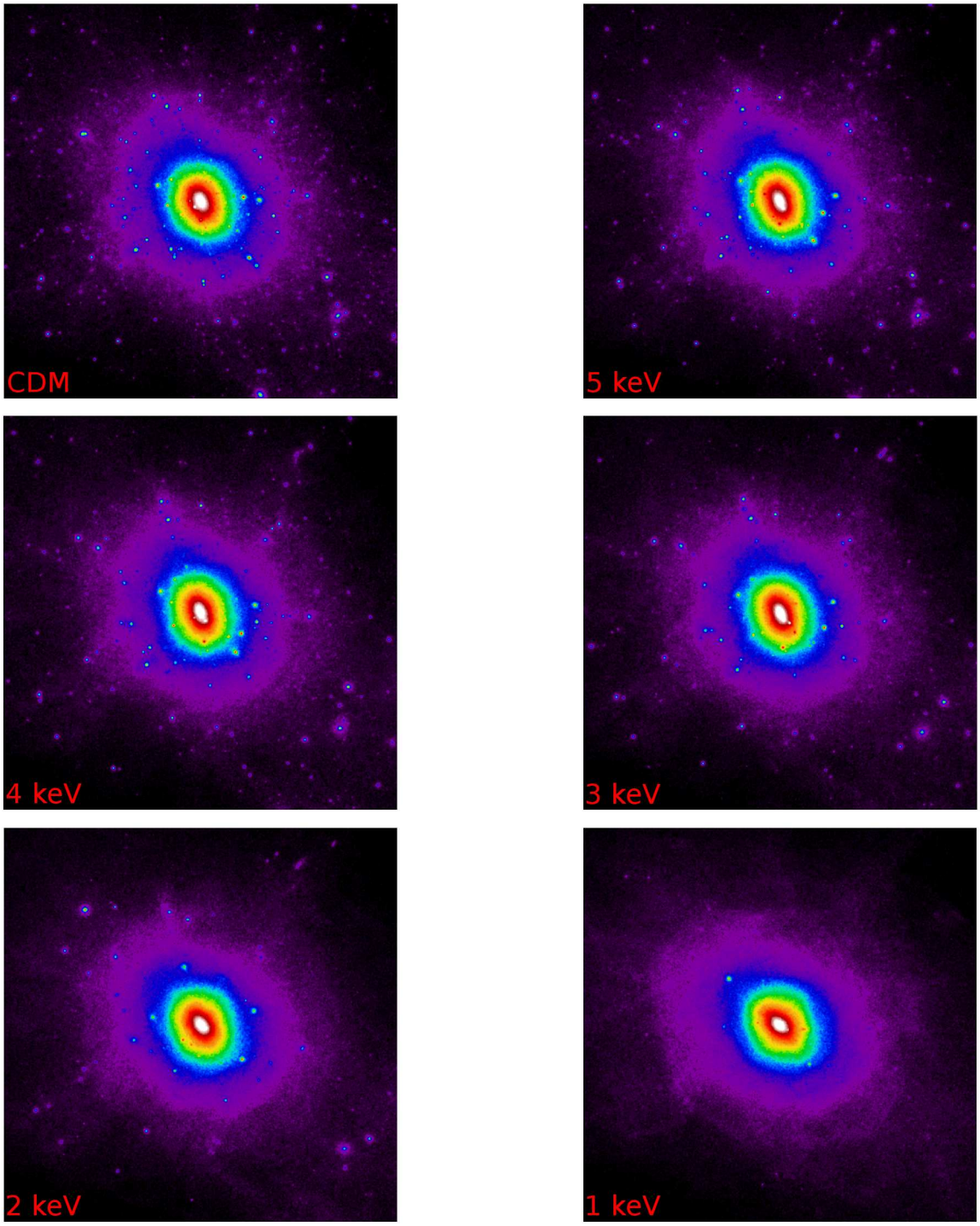

FIG. 4. Portraits of the simulated Milky Way halo at $z = 0$ in the *set B* low resolution simulations. Images are 1 Mpc on a side.

Ostriker [41] but were attributed to the fragmentation of matter filaments. The upturns occur at velocities that depend on the cosmology. For our warmest cosmology Poisson halos are important only at circular velocities less than about 6 km/s.

The vertical lines in Figure 7 show where $v_{max} =$ 8 km/s. Below this scale the high resolution CDM simulations begin to fall away from the Press-Schecter lines due to the resolution limits of the simulation. For $v_{max} > 8$ km/s our simulations are reasonably complete within R_{50} of each Milky Way although numerical destruction of a small fraction of satellites in the inner

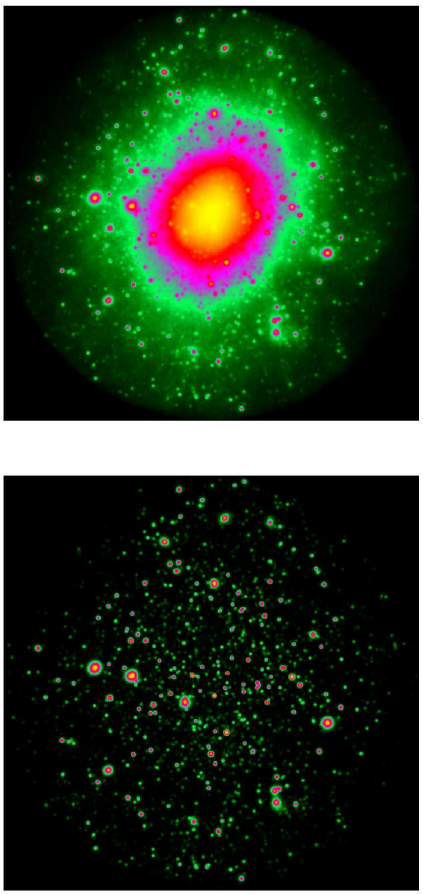

FIG. 5. Milky Way halo and satellites in the *set B* high resolution CDM simulation before (*top*) and after (*bottom*) subtracting the Milky Way profile. Only the satellites remain after subtraction. The halo was subtracted to a distance of 500 kpc from the Milky Way center.

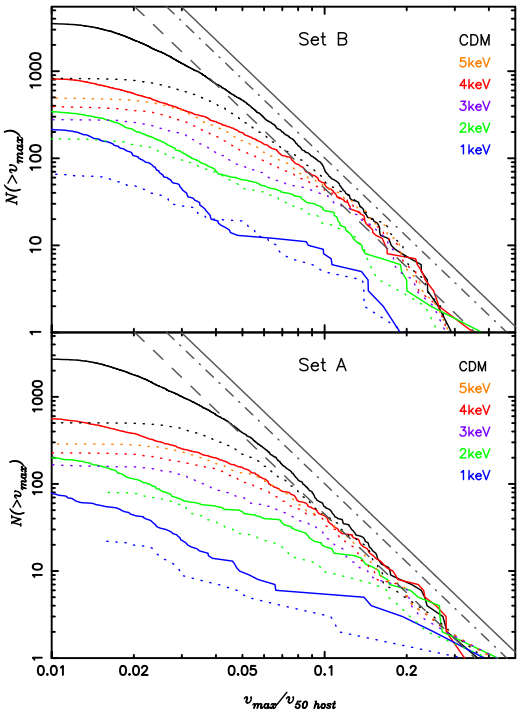

FIG. 6. Cumulative mass functions for satellites in our low (*dotted*) and high (*solid*) resolution *set B* (*top*) and *set* A (*bottom*) simulations. Satellite masses are characterized by their circular velocities and have been normalized to the circular velocity of the host halo at a radius enclosing an overdensity of 50. Straight sloped lines are the fitting formula from Via Lactea I, Via Lactea II, and the Aquarius simulations (*left to right*).

Milky Way wouldn't be apparent in Figure 7, especially for the CDM and 4 keV cosmologies. Before comparing our simulations to observations of the Milky Way we need to determine to what distance our simulations are convergent.

C. Convergence Study

Satellites orbiting in the halo of a larger galaxy are destroyed by tidal stripping and heating through encounters with other satellites. Satellites in simulations are also destroyed artificially by numerical effects that become dominant for poorly resolved halos in the inner halo region. There will therefore be a radius inside of which our simulations will not converge to a realistic representation of the actual Milky Way.

To determine the convergence of our simulations and have an idea of the variance of the results, we performed two simulations at lower and higher resolution and we also simulated two different realizations of a Milky Way-sized galaxy. We performed convergence studies following the argument elucidated below, in combination with results of published high resolution simulations found in the literature. Using the work of Moore et al., De Lucia et al., and Ishiyama et al. [2, 37, 43] we will assume that the shape of the cumulative satellite mass function for host halos of different masses is nearly constant and the total number of satellites scales linearly with the host mass. If the simulations are convergent the cumulative circular velocity function for satellites, $N(R)$, within a given Galactocentric radius, R, should be proportional to the enclosed mass, $M(R)$, and a function of R that represents the fraction of satellites that survive destruction from physical effects:

$$N(R) \equiv f(R)M(R), \tag{9}$$

where $f(R) \propto R^{\alpha}$. The normalization of $f(R)$ can be set using values of $N(R)$ and $M(R)$ at a distance R_0:

$$N(R)\left(\frac{R_0}{R}\right)^{\alpha}\left(\frac{M_0}{M(R)}\right) = N_0 = const. \tag{10}$$

The mass functions normalized in this way will be constant with radius where the simulations are convergent.

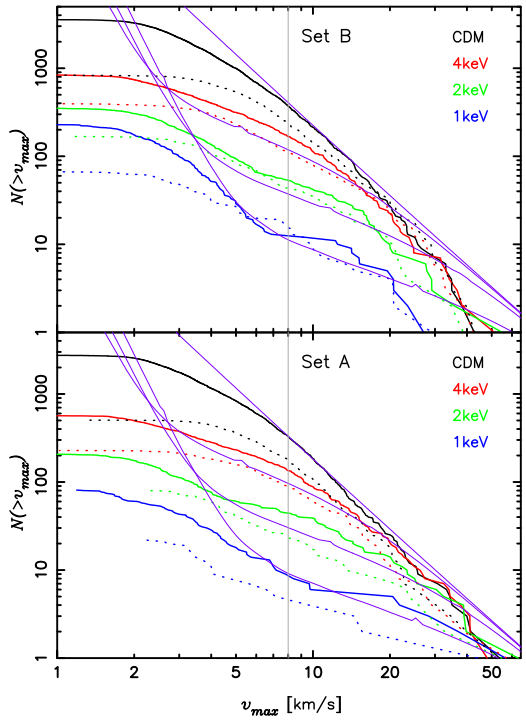

FIG. 7. Cumulative mass functions for satellites in our low (*dotted*) and high (*solid*) resolution *set B* (*top*) and *set A* (*bottom*) simulations. Mass functions calculated from Press-Schechter theory shifted vertically to match the CDM curves have been added. The WDM simulations are well fit by the theory. The addition of a constant power Poisson noise creates the upturns in the WDM cosmologies at velocites < 6 km/s. The level of Poisson noise was adjusted to match the upturn at 1 keV in *set B* but also matches the 2 keV well and the *set A* simulations. Below 8 km/s (vertical line) the CDM lines fall below the Press-Schechter calculations due to the resolution limits of the simulations.

Where numerical effects destroy satellites the mass functions will normalize to a lower value. We expect that α is constant because there isn't any characteristic scale for the destruction rate in dark matter only simulations. Hence, α can be determined at large radii where convergence is certain.

Figure 8 shows the normalized mass functions for the simulations. The normalization constants M_0, R_0 have been chosen at 200 kpc and the value of α (0.55) was adjusted by hand until a good fit was achieved for the *set B* mass functions above 200 kpc in the high resolution CDM cosmology at circular velocities > 8 km/s (vertical lines). This α also provides a good fit for the WDM cosmologies and for the *set A* simulations, although the 1 and 2 keV mass functions have a wider scatter due to the smaller numbers of satellites in these simulations. The $m_{WDM} = 4$ keV simulation is convergent for $v_{max} > 8$ km/s to distances > 100 kpc. At 75 kpc the effects of numerical resolution are apparent. The same value of α has been used in the normalization of the low resolution sets and appears to provide a good fit for the mass functions > 250 kpc (thin solid lines). The effects of numerical resolution on the destruction of satellites are apparent at larger distances in these simulations: < 200 kpc for CDM and < 150 kpc for WDM.

D. Comparison to Observations

Before the Sloan Digital Sky Survey there were only 12 classically known satellite galaxies to the Milky Way. Sixteen new satellites have been discovered in the SDSS, currently in Data Release 7. We list all known Milky Way satellites in Table II. We use the satellite distances given in Table II as their Galactocentric distances. When comparing the observed satellites to the simulations we must correct the SDSS dwarfs for completeness. The primary incompleteness of the SDSS is its sky coverage, 28.3% (11663 deg^2). Second, being a magnitude limited survey, the SDSS has a luminosity bias. The detection efficiency of dwarfs in the SDSS is a function of dwarf size, luminosity, distance, and Galactic latitude as shown by Walsh et al. [44]. An approximate expression is given in Tollerud et al. [45] (using the work of Koposov et al. [46]) for the distance which galaxies of luminosity $> L$ are completely detected: $d \approx 66\text{kpc}(L/1000\ L_\odot)^{1/2}$. Galaxies with $L > 10^4$ L$_\odot$ should be approximately complete to 200 kpc, with $L > 2300$ L$_\odot$ to 100 kpc. The distance range $100-200$ kpc is thus suited for comparisons because our simulations are convergent and the observations are nearly, but not quite, complete. For our analysis we will only use satellites with distances < 200 kpc. For comparison with the simulations we do a first order correction for the sky coverage of the SDSS assuming an isotropic distribution of satellites. The SDSS covers 0.283 of the sky so for every satellite detected we assume there are actually 3.54 satellites at that distance. Combined with the classic Milky Way satellites this forms our observed data set. We also implemented a conservative luminosity correction for the SDSS dwarfs using the formulas in Walsh et al. [44]. This adds 2 satellites making a total of 61 ± 13 satellites within 200 kpc where the error only includes Poisson statistics of the SDSS dwarfs: $3.54\sqrt{N_{SDSS}}$. The extra 2 satellites are at distances $150 - 200$ kpc and do not affect our conclusions. We note that we get the same result if we only include dwarfs detected in the Data Release 5 footprint and correct for the smaller sky coverage (8000 deg^2). We also note the formulas in Walsh et al. [44] assume the size-luminosity distribution of known dwarfs is representative of all satellites. There may be a population of dwarfs with surface brightnesses below the detection limit of the SDSS [62–65].

Willman 1 is an exceptional case in that it may not be a dark matter dominated dwarf galaxy but a globular cluster undergoing tidal disruption. Its size and luminosity are intermediate between Milky Way dwarfs and globular clusters [52]. Although it has a large metallicity spread unlike the stellar population of a globular cluster, when

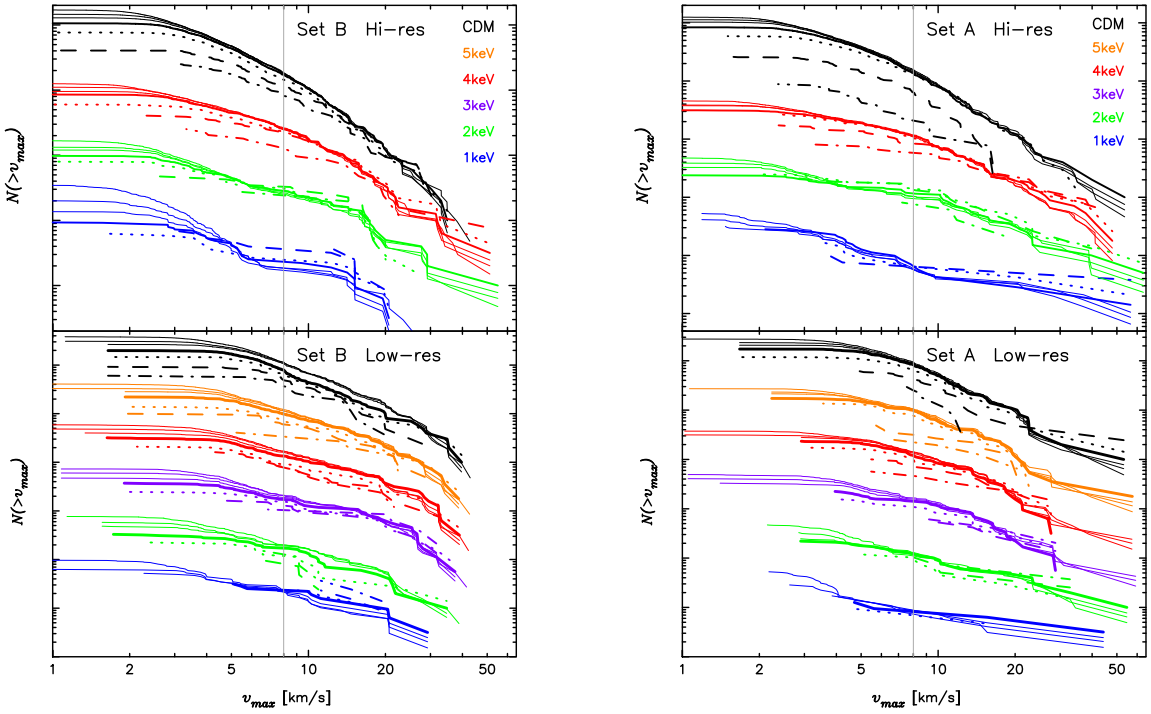

FIG. 8. *(Left).* Normalized mass functions for *set B* high (*top*) and low (*bottom*) resolution simulations. Thin solid lines are distances of 400, 300, and 250 kpc. Thick solid line is 200 kpc, dotted line is 150 kpc, dashed line is 100 kpc, dot-dashed line is 75 kpc. The WDM cosmologies have been shifted down vertically for clarity. The value $\alpha = 0.55$ was set by the high resolution simulation and provides good normalization for the low resolution as well but the effects of incompleteness become apparent at much larger radii ($150 - 200$ kpc compared to $75 - 100$ kpc for high res). *(Right).* Same as the left panel, but for the *set A* high (*top*) and low (*bottom*) resolution simulations. The value $\alpha = 0.55$ also provides good normalization for this set of halos.

deriving constraints on the dark matter particle mass we will consider both including and excluding Willman 1 as a Milky Way satellite.

When comparing observations and simulations we need to know the maximum circular velocities of the dark matter halos the observed galaxies are presumably embedded in. Ricotti & Gnedin [62] found in simulations that the maximum circular velocities of satellites are at least twice the velocity dispersion of the stellar component. Assuming the stellar velocity dispersions of the observed dwarfs are $\sqrt{3}$ times the line-of-sight velocity dispersions (σ_{star} in Table II), then all dwarfs with measured velocity dispersions have max circular velocities greater than 8 km/s. We assume dwarfs without measured velocity dispersions are similar to the other known dwarfs and conservatively conclude all dwarfs reside in dark matter halos with max circular velocities greater than 8 km/s. An alternative approach is the work of Wolf et al. [66] relating the circular velocity at half light radius to σ_{star}: $v_c(r_{1/2}) = \sqrt{3}\sigma_{star}$. All the observed dwarfs except Leo V have circular velocities at half light radius about 6 km/s or greater. Since the max circular velocity must be greater than or equal to the half light circular velocity we will also consider that all observed dwarfs reside in halos with $v_{max} > 6$ km/s.

In the left panel of Figure 9 we plot histograms of the number of satellites with distance for the observed and simulation data sets with an 8 km/s max circular velocity cut. The upward arrows on the observed data bars indicate these are only lower limits due to the surface brightness limits of the SDSS, it is possible there are more dwarfs yet to be discovered. The 8 km/s cut to the simulation data avoids Poisson halos and assures the high resolution simulations are complete to at least $r = 100$ kpc. The low resolution simulations are also plotted in these figures but they are complete only to 150 kpc. Focusing on the $100 - 200$ kpc bins it is clear the 1 keV has far too few satellites to match the observations. The 2 keV simulations can be consistent with the observations if the simulations are incomplete below 100 kpc or the sky correction has overestimated the number of satellites in the inner Milky Way. The 4 keV simulations can also be consistent with the observations although they may require some of the dark matter halos to not host luminous galaxies. It is not clear from this plot how variance in the satellite abundances for the simulated halos may affect the results.

The number of satellites in the simulations can be corrected for completeness using the convergence equation, Eq. (10). We used the mass and number of satellites inside R_{50} for the normalization and calculated the number of satellites in 50 kpc bins for the high resolution simulations. The results are shown in the right panel of Figure 9. The results are very similar across cosmolo-

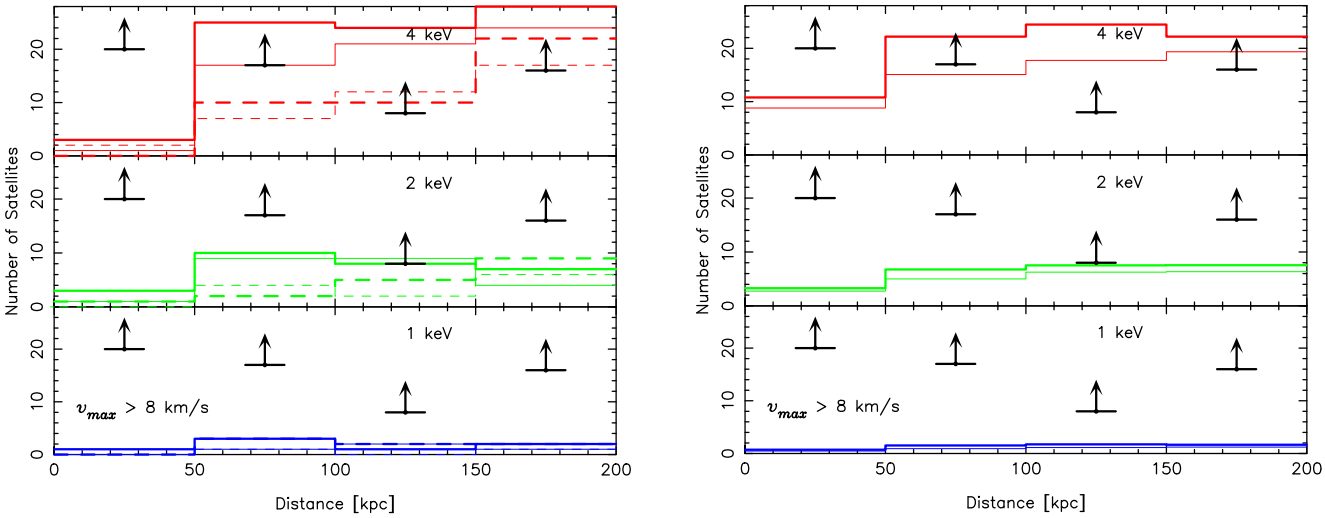

FIG. 9. *(Left)* Number of satellites with distance from the Milky Way grouped into 50 kpc bins. The simulation satellites have been cut by circular velocity > 8 km/s. Solid lines show the data from the high resolution and dashed lines show the low resolution simulations, thick lines are the *set B* simulations. The bars with arrows are the observed satellites after correcting for the sky coverage of the SDSS. Observations are incomplete at distances greater than about $50-100$ kpc (depending on the lumiosity and surface brightness of the dwarf), while simulations have not converged for less than about 100 kpc for high resolution and 150 kpc for low resolution. *(Right)* Number of satellites with distance from the Milky Way like the plot at left but calculated from the convergence equation (Eq. 10). The convergence correction affects mainly the 4 keV $0-50$ kpc bin.

gies, a nearly constant number of satellites per bin from $50-200$ kpc with about half as many in the $0-50$ kpc bin. The plots are also very similar to the simulation data plots except for the $0-50$ kpc bin in the 4 keV cosmology where about 10 satellites were destroyed by numerical effects. The $0-50$ kpc bin is most important for constraining the dark matter particle mass because the observations are most complete in this bin.

In Figure 10 we plot the number of satellites in the $0-50$ kpc bin calculated from the convergence equation for the high resolution *set B* Milky Way as a function of the particle mass. To account for the variance in satellite abundances we also scale to the Aquarius and Via Lactea I simulations (shaded region). We assume the Aquarius abundances represent the upper limit for the Milky Way since these simulations have the largest abundances of published Milky Way-sized dark matter halos that also host spiral galaxies or are isolated and therefore likely to host spirals. Some of the halos in Ishiyama et al. [37] have higher abundances but they are also undergoing major mergers and not representative of the Milky Way. The solid horizontal line shows the number of observed satellites after applying sky coverage corrections to the SDSS data while the dashed horizontal lines show the 68% and 95% confidence lower limits and the raw number of observed satellites without any correction. From the corrected observations we get $m_{WDM} > 3.7$ keV with > 3.2 keV at 68% confidence and > 2.6 keV at 95% confidence. The raw observed line is an extremely conservative limit as the number of Milky Way satellites within 50 kpc is almost certainly greater than 7, but it sets an absolute lower limit of $m_{WDM} > 2$ keV.

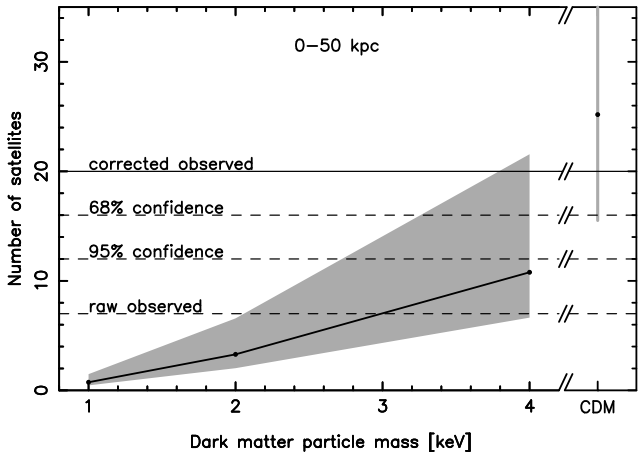

FIG. 10. Number of satellites from 0-50 kpc calculated from the convergence equation in the *set B* high resolution simulations for $v_{max} > 8$ km/s (thick line with points) compared to the observed number of Milky Way satellites, including Willman 1, with corrections (solid horizontal line) and without ("raw") and at 68% and 95% confidence (dashed horizontal lines). The gray shaded area is the simulation data scaled to the satellite abundances of the Aquarius simulations at the high end and Via Lactea I on the low end. The uncorrected observations intersect the shaded region at $m_{WDM} = 2$ keV, this is an extremely conservative lower limit on the dark matter particle mass.

We repeated the same analysis using a 6 km/s max circular velocity cut to the simulation data. We also considered the effects when Willman 1 was excluded from

TABLE II. Summary of known Milky Way satellites.

Name	*dist* [kpc]	σ_{star} [km/s]	M_V	References
Classical (pre-SDSS)				
Sagittar	24 ± 2	11.4 ± 0.7	-13.4	[47]
LMC	49 ± 2	-	-18.4	[47]
SMC	58 ± 2	-	-17.0	[47]
Ursa Minor	66 ± 3	9.3 ± 1.8	-8.9	[47]
Draco	79 ± 4	9.5 ± 1.6	-8.8	[47]
Sculptor	79 ± 4	6.6 ± 0.7	-11.1	[47]
Sextans	86 ± 4	6.6 ± 0.7	-9.5	[47]
Carina	94 ± 5	6.8 ± 1.6	-9.3	[47]
Fornax	138 ± 8	10.5 ± 1.5	-13.2	[47]
Leo II	205 ± 12	6.7 ± 1.1	-9.6	[47]
Leo I	270 ± 30	8.8 ± 0.9	-11.9	[47]
Phoenix	405 ± 15	-	-10.1	[47]
SDSS discovered				
Segue I	23 ± 2	4.3 ± 1.2	-1.5	[48]
Ursa Major II	30 ± 5	6.7 ± 1.4	-3.8	[49, 50]
Segue II	~ 35	3.4 ± 2.0	-2.5	[51]
Willman I	38 ± 7	$4.3^{+2.3}_{-1.3}$	-2.5	[49, 52]
Coma Berenics	44 ± 4	4.6 ± 0.8	-3.7	[50, 53]
Bootes II	60 ± 10	-	-3.1	[54]
Bootes I	62 ± 3	$6.5^{+2.0}_{-1.4}$	-5.8	[49]
Pisces I	80 ± 14	-	-	[55, 56]
Ursa Major I	106^{+9}_{-8}	7.6 ± 1.0	-5.6	[50]
Hercules	140^{+13}_{-12}	5.1 ± 0.9	-6.0	[50, 53]
Canes Venatici II	150^{+15}_{-14}	4.6 ± 1.0	-4.8	[50, 53]
Leo IV	160^{+15}_{-14}	3.3 ± 1.7	-5.8	[50, 53]
Leo V	175 ± 9	2.4 ± 1.8	-5.2	[57, 58]
Pisces II	~ 180	-	-5.0	[59]
Canes Venatici I	220^{+25}_{-16}	7.6 ± 0.4	-7.9	[50, 60]
Leo T	~ 420	7.5 ± 1.6	-7.1	[50, 61]

the observed data set for both the 6 km/s and 8 km/s analysis. We present the results in Table III. In the most conservative case, where Willman 1 is not a dark matter dominated dwarf galaxy and all observed satellites correspond to dark matter halos with max circular velocities > 6 km/s, we can say $m_{WDM} > 2.1$ keV with 95% confidence. We adopt this as our formal limit for this work.

TABLE III. Dark matter particle mass constraints (in keV) for simulated halo max circular velocity cuts of 8 and 6 km/s and including or excluding Willman 1 from the observed data set.

	$v_{max} > 8$ km/s		$v_{max} > 6$ km/s	
Willman 1?	Included	Excluded	Included	Excluded
raw observed	> 2.0	> 1.9	> 1.8	> 1.6
95% confidence	> 2.6	> 2.3	> 2.3	> 2.1
68% confidence	> 3.2	> 2.6	> 2.6	> 2.3
sky corrected	> 3.7	> 3.2	> 3.0	> 2.6

IV. DISCUSSION

We found in the preceding section a conservative lower limit of $m_{WDM} > 2.1$ keV on the dark matter particle mass. We also found the 1 keV WDM simulation has too few satellites to match the Milky Way observations. This agrees with the semi-analytic modeling and Milky Way satellite luminosity functions in WDM cosmologies work of Macciò & Fontanot [8].

Our result can also be compared to limits on the particle mass from the Lyman-α forest in high redshift quasars. Lyman-α absorption by neutral hydrogen along the line of sight to distant quasars over redshifts 2–6 probes the matter power spectrum in the mildly nonlinear regime on scales 1–80 Mpc/h. Viel et al. [20, 67, 68] have numerically modeled the Lyman-α forest flux power spectra for varied cosmological parameters and compared to observed quasar forests to obtain lower limits on the dark matter particle mass. Their 2006 work used low resolution spectra for 3035 quasars ($2.2 < z < 4.2$) from the SDSS [69] and found a 2σ lower limit of 2 keV for a thermal WDM particle. This limit agrees with our results that a 2.1 keV particle is the lower limit that can reproduce the observed number of Milky Way satellites. However, their latest work [68] uses high resolution spectra for 55 quasars ($2.0 < z < 6.4$) from the Keck HIRES spectrograph in addition to the SDSS quasars. With the new data they report a lower limit of 4 keV (2σ). A caveat arises in Viel et al. [70] who show the flux power spectrum from the SDSS data prefer larger values of the intergalactic medium (IGM) temperature at mean density than expected from photoionization. The flux power spectrum temperature is also higher than that derived from an analysis of the flux probability distribution function of 18 high resolution spectra from UVES/VLT and also higher than constraints from the widths of thermally broadened absorption lines [71, 72]. This could be explained by an unaccounted for systematic error in the SDSS flux power spectrum data which may also affect the derived dark matter particle mass limits.

Using the scaling relation for sterile neutrinos we find a lower limit $m_s > 11.8$ keV with 95% confidence for a DW produced sterile neutrino particle. Scaling to the other production mechanisms we get $m_s > 7.9$ keV for the SF mechanism and $m_s > 2.6$ keV for Higgs decay sterile neutrinos. Sterile neutrinos are expected to radiatively decay to a photon and a lighter mass neutrino. This decay should produce an X-ray spectral line with energy $E_\gamma = m_s/2$. Abazajian et al. [73] used *Chandra* spectra of the the unresolved component of the cosmic X-

ray background in the *Chandra* Deep Fields North and South to search for a contribution from the decay of sterile neutrinos in the dark matter halo of the Milky Way. Their non-detection places an upper limit on the sterile neutrino mass that depends on the model for the Milky Way halo. Using their lowest mass models they adopt a conservative limit of $m_s < 5.7$ keV (2σ). Our lower limit for DW and SF produced neutrinos is significantly above the X-ray upper limit implying the dark matter is not made entirely of sterile neutrinos produced by these mechanisms. If sterile neutrinos compose only part of the dark matter the X-ray upper mass limit can be higher but our lower mass limits do not necessarily apply to mixed dark matter cosmologies. Higgs decay produced sterile neutrinos can, however, constitute all the dark matter and be consistent with the X-ray and Milky Way satellite constraints. These conclusions agree with the results of *Suzaku* observations of Ursa Minor [74].

V. SUMMARY

We have conducted N-body simulations of the formation of a Milky Way-sized dark matter halo in CDM and WDM cosmologies. Such simulations are complicated by the formation of nonphysical small mass halos due to the discreteness of the initial conditions. We have shown that these halos can be modeled by including Poisson noise in Press-Schechter calculations and some do survive to end up inside the halo of the Milky Way but with sufficient resolution they are only important at small scales and can be avoided with an appropriate circular velocity or mass cut.

We have studied the number of satellite halos as a function of distance from the Milky Way. The 4 keV and 2 keV WDM simulations can adequately reproduce the observed number of satellites at hundreds of kiloparsecs while the 1 keV is severely deficient. Correcting our simulations for numerical destruction in the inner 50 kpc and scaling to the higher satellite abundances of the Aquarius simulations, we find a very conservative lower limit of > 2.1 keV at 95% confidence. This agrees with the earlier Lyman-α forest modeling work of Viel et al. [67] that $m_{WDM} > 2$ keV but the two methods are independent and almost certainly are subject to different systematic errors if any exist. Their latest work [68] raises the limit to $m_{WDM} > 4$ keV but problems with the derived IGM temperature and mean density may indicate the SDSS spectra they used suffer a systematic error [70].

Our lower limit of 2.1 keV for a thermal dark matter particle scales to lower limits of 11.8, 7.9, 2.6 keV for DW, SF, and Higgs decay produced sterile neutrinos. Sterile neutrinos, if they exist, are expected to decay into X-rays and active neutrinos. Observations of the unresolved cosmic X-ray background combined with models of the Milky Way halo set an upper limit of 5.7 keV on the mass of the sterile neutrino [73], assuming they constitute 100% of the dark matter. Sterile neutrinos are viable dark matter candidates but if they are produced by the DW or SF mechanisms they cannot account for all the dark matter.

Our simulations followed the formation of two Milky Way-sized halos in CDM and WDM cosmologies. Numerical simulations show significant variance (100%) in the number of satellites in Milky Way-sized halos, an effect that can be easily quantified using published studies and incorporated in our results. To account for the effect of variance we counted satellites in 50 kpc bins and scaled our abundances to the larger values of the Aquarius simulation suite which were selected, using semi-analytic modeling, to host Milky Way-type spiral galaxies and showed $< 10\%$ variance in their number of satellites. Our constraint is a conservative lower limit since we only correct the number of SDSS dwarfs for sky completeness. An analysis that takes into account the surface brightness limits of the observational data may allow tighter constraints however the analysis would be somewhat model dependent.

We have demonstrated how N-body simulations of the Milky Way and its satellites can set limits on the dark matter particle mass comparable to complementary methods such as modeling the Lyman-α forest. These limits are helped greatly by the discovery of many new Milky Way satellites in the SDSS. There may still be a population of low luminosity, low surface brightness dwarf galaxies undetectable by the SDSS [62–65]. Future surveys like LSST, DES, PanSTARRS, and SkyMapper have the potential to discover many more Milky Way satellites and further improve constraints on the mass of the dark matter particle.

ACKNOWLEDGMENTS

It is our pleasure to thank Alexander Kusenko and Kev Abazajian for helpful discussions. Emil Polisensky acknowledges support under the Edison Memorial Graduate Training Program at the Naval Research Laboratory.

[1] A. Klypin, A. V. Kravtsov, O. Valenzuela, and F. Prada, Astrophys. J. **522**, 82 (Sep. 1999), arXiv:astro-ph/9901240.

[2] B. Moore, S. Ghigna, F. Governato, G. Lake, T. Quinn, J. Stadel, and P. Tozzi, Astrophys. J. Lett. **524**, L19 (Oct. 1999), arXiv:astro-ph/9907411.

[3] P. Colín, V. Avila-Reese, and O. Valenzuela, Astrophys. J. **542**, 622 (Oct. 2000), arXiv:astro-ph/0004115.

[4] V. Avila-Reese, P. Colín, O. Valenzuela, E. D'Onghia,

and C. Firmani, Astrophys. J. **559**, 516 (Oct. 2001), arXiv:astro-ph/0010525.
[5] P. Bode, J. P. Ostriker, and N. Turok, Astrophys. J. **556**, 93 (Jul. 2001), arXiv:astro-ph/0010389.
[6] A. Knebe, J. E. G. Devriendt, A. Mahmood, and J. Silk, Mon. Not. R. Astron. Soc. **329**, 813 (Feb. 2002), arXiv:astro-ph/0105316.
[7] A. Knebe, J. E. G. Devriendt, B. K. Gibson, and J. Silk, Mon. Not. R. Astron. Soc. **345**, 1285 (Nov. 2003), arXiv:astro-ph/0302443.
[8] A. V. Maccio' and F. Fontanot, ArXiv e-prints(Oct. 2009), arXiv:0910.2460.
[9] A. L. Melott, ArXiv e-prints(Sep. 2007), arXiv:0709.0745.
[10] J. Wang and S. D. M. White, Mon. Not. R. Astron. Soc. **380**, 93 (Sep. 2007), arXiv:astro-ph/0702575.
[11] F. J. Castander, Astrophys. Space Sci. **263**, 91 (Jun. 1998).
[12] V. Springel, Mon. Not. R. Astron. Soc. **364**, 1105 (Dec. 2005), arXiv:astro-ph/0505010.
[13] D. N. Spergel, R. Bean, O. Doré, M. R. Nolta, C. L. Bennett, J. Dunkley, G. Hinshaw, N. Jarosik, E. Komatsu, L. Page, H. V. Peiris, L. Verde, M. Halpern, R. S. Hill, A. Kogut, M. Limon, S. S. Meyer, N. Odegard, G. S. Tucker, J. L. Weiland, E. Wollack, and E. L. Wright, Astrophys. J. Suppl. **170**, 377 (Jun. 2007), arXiv:astro-ph/0603449.
[14] E. Bertschinger, Astrophys. J. Suppl. **137**, 1 (Nov. 2001), arXiv:astro-ph/0103301.
[15] J. M. Bardeen, J. R. Bond, N. Kaiser, and A. S. Szalay, Astrophys. J. **304**, 15 (May 1986).
[16] D. J. Eisenstein and W. Hu, Astrophys. J. **496**, 605 (Mar. 1998), arXiv:astro-ph/9709112.
[17] A. Kusenko, Physics Reports **481**, 1 (Sep. 2009), arXiv:0906.2968.
[18] S. Dodelson and L. M. Widrow, Physical Review Letters **72**, 17 (Jan. 1994), arXiv:hep-ph/9303287.
[19] K. Abazajian, Phys. Rev. D **73**, 063513 (Mar. 2006), arXiv:astro-ph/0512631.
[20] M. Viel, J. Lesgourgues, M. G. Haehnelt, S. Matarrese, and A. Riotto, Phys. Rev. D **71**, 063534 (Mar. 2005), arXiv:astro-ph/0501562.
[21] X. Shi and G. M. Fuller, Physical Review Letters **82**, 2832 (Apr. 1999), arXiv:astro-ph/9810076.
[22] A. Kusenko, Physical Review Letters **97**, 241301 (Dec. 2006), arXiv:hep-ph/0609081.
[23] M. Kamionkowski and A. R. Liddle, Physical Review Letters **84**, 4525 (May 2000), arXiv:astro-ph/9911103.
[24] K. Sigurdson and M. Kamionkowski, Physical Review Letters **92**, 171302 (Apr. 2004), arXiv:astro-ph/0311486.
[25] M. Kaplinghat, Phys. Rev. D **72**, 063510 (Sep. 2005), arXiv:astro-ph/0507300.
[26] D. J. Eisenstein and P. Hut, Astrophys. J. **498**, 137 (May 1998), arXiv:astro-ph/9712200.
[27] C. Power, J. F. Navarro, A. Jenkins, C. S. Frenk, S. D. M. White, V. Springel, J. Stadel, and T. Quinn, Mon. Not. R. Astron. Soc. **338**, 14 (Jan. 2003), arXiv:astro-ph/0201544.
[28] J. M. Gelb and E. Bertschinger, Astrophys. J. **436**, 467 (Dec. 1994), arXiv:astro-ph/9408028.
[29] J. Stadel, http://www-hpcc.astro.washington.edu/tools/skid2 (2000).
[30] D. H. Weinberg, L. Hernquist, and N. Katz, Astrophys. J. **477**, 8 (Mar. 1997), arXiv:astro-ph/9604175.
[31] J. Diemand, M. Kuhlen, and P. Madau, Astrophys. J. **649**, 1 (Sep. 2006), arXiv:astro-ph/0603250.
[32] J. Diemand, M. Kuhlen, and P. Madau, Astrophys. J. **657**, 262 (Mar. 2007), arXiv:astro-ph/0611370.
[33] S. R. Knollmann and A. Knebe, Astrophys. J. Suppl. **182**, 608 (Jun. 2009), arXiv:0904.3662.
[34] V. Springel, S. D. M. White, G. Tormen, and G. Kauffmann, Mon. Not. R. Astron. Soc. **328**, 726 (Dec. 2001), arXiv:astro-ph/0012055.
[35] J. Diemand, M. Kuhlen, P. Madau, M. Zemp, B. Moore, D. Potter, and J. Stadel, Nature (London) **454**, 735 (Aug. 2008), arXiv:0805.1244.
[36] V. Springel, J. Wang, M. Vogelsberger, A. Ludlow, A. Jenkins, A. Helmi, J. F. Navarro, C. S. Frenk, and S. D. M. White, Mon. Not. R. Astron. Soc. **391**, 1685 (Dec. 2008), arXiv:0809.0898.
[37] T. Ishiyama, T. Fukushige, and J. Makino, Astrophys. J. **696**, 2115 (May 2009), arXiv:0812.0683.
[38] P. J. Quinn and J. Goodman, Astrophys. J. **309**, 472 (Oct. 1986).
[39] I. R. Walker, J. C. Mihos, and L. Hernquist, Astrophys. J. **460**, 121 (Mar. 1996), arXiv:astro-ph/9510052.
[40] W. H. Press and P. Schechter, Astrophys. J. **187**, 425 (Feb. 1974).
[41] R. Barkana, Z. Haiman, and J. P. Ostriker, Astrophys. J. **558**, 482 (Sep. 2001), arXiv:astro-ph/0102304.
[42] N. Afshordi, P. McDonald, and D. N. Spergel, Astrophys. J. Lett. **594**, L71 (Sep. 2003), arXiv:astro-ph/0302035.
[43] G. De Lucia, G. Kauffmann, V. Springel, S. D. M. White, B. Lanzoni, F. Stoehr, G. Tormen, and N. Yoshida, Mon. Not. R. Astron. Soc. **348**, 333 (Feb. 2004), arXiv:astro-ph/0306205.
[44] S. M. Walsh, B. Willman, and H. Jerjen, Astron. J. **137**, 450 (Jan. 2009), arXiv:0807.3345.
[45] E. J. Tollerud, J. S. Bullock, L. E. Strigari, and B. Willman, Astrophys. J. **688**, 277 (Nov. 2008), arXiv:0806.4381.
[46] S. Koposov, V. Belokurov, N. W. Evans, P. C. Hewett, M. J. Irwin, G. Gilmore, D. B. Zucker, H. Rix, M. Fellhauer, E. F. Bell, and E. V. Glushkova, Astrophys. J. **686**, 279 (Oct. 2008), arXiv:0706.2687.
[47] M. L. Mateo, Ann. Rev. Astron. Astrophys. **36**, 435 (1998), arXiv:astro-ph/9810070.
[48] M. Geha, B. Willman, J. D. Simon, L. E. Strigari, E. N. Kirby, D. R. Law, and J. Strader, Astrophys. J. **692**, 1464 (Feb. 2009), arXiv:0809.2781.
[49] N. F. Martin, R. A. Ibata, S. C. Chapman, M. Irwin, and G. F. Lewis, Mon. Not. R. Astron. Soc. **380**, 281 (Sep. 2007), arXiv:0705.4622.
[50] J. D. Simon and M. Geha, Astrophys. J. **670**, 313 (Nov. 2007), arXiv:0706.0516.
[51] V. Belokurov, M. G. Walker, N. W. Evans, G. Gilmore, M. J. Irwin, M. Mateo, L. Mayer, E. Olszewski, J. Bechtold, and T. Pickering, Mon. Not. R. Astron. Soc. **397**, 1748 (Aug. 2009), arXiv:0903.0818.
[52] B. Willman, M. R. Blanton, A. A. West, J. J. Dalcanton, D. W. Hogg, D. P. Schneider, N. Wherry, B. Yanny, and J. Brinkmann, Astron. J. **129**, 2692 (Jun. 2005), arXiv:astro-ph/0410416.
[53] V. Belokurov, D. B. Zucker, N. W. Evans, J. T. Kleyna,

S. Koposov, S. T. Hodgkin, M. J. Irwin, G. Gilmore, M. I. Wilkinson, M. Fellhauer, D. M. Bramich, P. C. Hewett, S. Vidrih, J. T. A. De Jong, J. A. Smith, H. Rix, E. F. Bell, R. F. G. Wyse, H. J. Newberg, P. A. Mayeur, B. Yanny, C. M. Rockosi, O. Y. Gnedin, D. P. Schneider, T. C. Beers, J. C. Barentine, H. Brewington, J. Brinkmann, M. Harvanek, S. J. Kleinman, J. Krzesinski, D. Long, A. Nitta, and S. A. Snedden, Astrophys. J. **654**, 897 (Jan. 2007), arXiv:astro-ph/0608448.

[54] S. M. Walsh, H. Jerjen, and B. Willman, Astrophys. J. Lett. **662**, L83 (Jun. 2007), arXiv:0705.1378.

[55] L. L. Watkins, N. W. Evans, V. Belokurov, M. C. Smith, P. C. Hewett, D. M. Bramich, G. F. Gilmore, M. J. Irwin, S. Vidrih, Ł. Wyrzykowski, and D. B. Zucker, Mon. Not. R. Astron. Soc. **398**, 1757 (Oct. 2009), arXiv:0906.0498.

[56] J. A. Kollmeier, A. Gould, S. Shectman, I. B. Thompson, G. W. Preston, J. D. Simon, J. D. Crane, Ž. Ivezić, and B. Sesar, Astrophys. J. Lett. **705**, L158 (Nov. 2009), arXiv:0908.1381.

[57] J. T. A. de Jong, N. F. Martin, H. Rix, K. W. Smith, S. Jin, and A. V. Maccio', ArXiv e-prints(Dec. 2009), arXiv:0912.3251.

[58] V. Belokurov, M. G. Walker, N. W. Evans, D. C. Faria, G. Gilmore, M. J. Irwin, S. Koposov, M. Mateo, E. Olszewski, and D. B. Zucker, Astrophys. J. Lett. **686**, L83 (Oct. 2008), arXiv:0807.2831.

[59] V. Belokurov, M. G. Walker, N. W. Evans, G. Gilmore, M. J. Irwin, D. Just, S. Koposov, M. Mateo, E. Olszewski, L. Watkins, and L. Wyrzykowski, Astrophys. J. Lett. **712**, L103 (Mar. 2010), arXiv:1002.0504.

[60] D. B. Zucker, V. Belokurov, N. W. Evans, M. I. Wilkinson, M. J. Irwin, T. Sivarani, S. Hodgkin, D. M. Bramich, J. M. Irwin, G. Gilmore, B. Willman, S. Vidrih, M. Fellhauer, P. C. Hewett, T. C. Beers, E. F. Bell, E. K. Grebel, D. P. Schneider, H. J. Newberg, R. F. G. Wyse, C. M. Rockosi, B. Yanny, R. Lupton, J. A. Smith, J. C. Barentine, H. Brewington, J. Brinkmann, M. Harvanek, S. J. Kleinman, J. Krzesinski, D. Long, A. Nitta, and S. A. Snedden, Astrophys. J. Lett. **643**, L103 (Jun. 2006), arXiv:astro-ph/0604354.

[61] M. J. Irwin, V. Belokurov, N. W. Evans, E. V. Ryan-Weber, J. T. A. de Jong, S. Koposov, D. B. Zucker, S. T. Hodgkin, G. Gilmore, P. Prema, L. Hebb, A. Begum, M. Fellhauer, P. C. Hewett, R. C. Kennicutt, Jr., M. I. Wilkinson, D. M. Bramich, S. Vidrih, H. Rix, T. C. Beers, J. C. Barentine, H. Brewington, M. Harvanek, J. Krzesinski, D. Long, A. Nitta, and S. A. Snedden, Astrophys. J. Lett. **656**, L13 (Feb. 2007), arXiv:astro-ph/0701154.

[62] M. Ricotti and N. Y. Gnedin, Astrophys. J. **629**, 259 (Aug. 2005), arXiv:astro-ph/0408563.

[63] M. Ricotti, N. Y. Gnedin, and J. M. Shull, Astrophys. J. **685**, 21 (Sep. 2008), arXiv:0802.2715.

[64] M. Ricotti, Advances in Astronomy **2010** (2010), doi: "bibinfo doi 10.1155/2010/271592, arXiv:0911.2792.

[65] M. S. Bovill and M. Ricotti, Astrophys. J. **693**, 1859 (Mar. 2009), arXiv:0806.2340.

[66] J. Wolf, G. D. Martinez, J. S. Bullock, M. Kaplinghat, M. Geha, R. R. Munoz, J. D. Simon, and F. F. Avedo, ArXiv e-prints(Aug. 2009), arXiv:0908.2995.

[67] M. Viel, J. Lesgourgues, M. G. Haehnelt, S. Matarrese, and A. Riotto, Physical Review Letters **97**, 071301 (Aug. 2006), arXiv:astro-ph/0605706.

[68] M. Viel, G. D. Becker, J. S. Bolton, M. G. Haehnelt, M. Rauch, and W. L. W. Sargent, Physical Review Letters **100**, 041304 (Feb. 2008), arXiv:0709.0131.

[69] P. McDonald, U. Seljak, S. Burles, D. J. Schlegel, D. H. Weinberg, R. Cen, D. Shih, J. Schaye, D. P. Schneider, N. A. Bahcall, J. W. Briggs, J. Brinkmann, R. J. Brunner, M. Fukugita, J. E. Gunn, Ž. Ivezić, S. Kent, R. H. Lupton, and D. E. Vanden Berk, Astrophys. J. Suppl. **163**, 80 (Mar. 2006), arXiv:astro-ph/0405013.

[70] M. Viel, J. S. Bolton, and M. G. Haehnelt, Mon. Not. R. Astron. Soc. **399**, L39 (Oct. 2009), arXiv:0907.2927.

[71] M. Ricotti, N. Y. Gnedin, and J. M. Shull, Astrophys. J. **534**, 41 (May 2000), arXiv:astro-ph/9906413.

[72] J. Schaye, T. Theuns, M. Rauch, G. Efstathiou, and W. L. W. Sargent, Mon. Not. R. Astron. Soc. **318**, 817 (Nov. 2000), arXiv:astro-ph/9912432.

[73] K. N. Abazajian, M. Markevitch, S. M. Koushiappas, and R. C. Hickox, Phys. Rev. D **75**, 063511 (Mar. 2007), arXiv:astro-ph/0611144.

[74] M. Loewenstein, A. Kusenko, and P. L. Biermann, Astrophys. J. **700**, 426 (Jul. 2009), arXiv:0812.2710.

Appendix

We used the BBKS formula for the CDM transfer function when generating the initial conditions for our simulations. This formula assumes a baryon density of zero. Eisenstein & Hu [16] calculated transfer functions for CDM cosmologies that include baryon physics. We plot the power spectra for the fitting formula of Eisenstein & Hu (with $\Omega_b = 0.04$) and BBKS in the left panel of Figure 11 which shows that, for a fixed value of σ_8, BBKS underestimates power on scales $k \lesssim 0.1$ but the power spectra are nearly identical for scales $\lesssim 14$ Mpc. With $\Omega_m = 0.238$ a Milky Way-sized halo with mass $\sim 2 \times 10^{12}$ $M_\odot$ would form from a spherical region with diameter 4.8 Mpc ($k = 0.28$ h/Mpc). This scale is well in the region where the power spectra are nearly equal and we would not expect the use of BBKS to bias our results.

To check if BBKS might affect the number of satellites we reran the *set B* low resolution CDM, 1 keV WDM, 2 keV WDM, and high resolution CDM simulations using initial conditions generated from the formula of Eisenstein & Hu. The right panel of Figure 11 compares the mass function of satellites. The results are in good agreement and we conclude that the use of BBKS has not introduced a systematic error into our results.

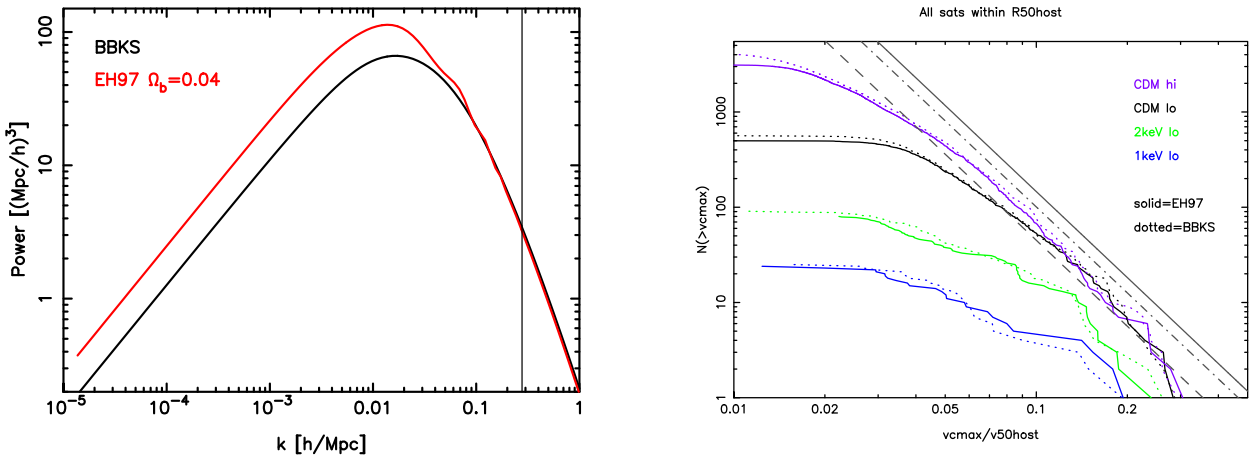

FIG. 11. *Left* Comparison of CDM power spectra calculated from the fitting formula of BBKS and Eisenstein & Hu (EH97). On scales $k > 0.1$ h/Mpc (< 14 Mpc) the power spectra are nearly identical. The vertical line is the diameter of a spherical region with density $\Omega_m \rho_c$ enclosing a Milky Way-sized mass 2×10^{12} $M_\odot$ (~ 5 Mpc). This scale is well within the range where the power spectra are nearly equal. *(Right)* Mass function comparison for *set B* simulations using fitting formula for CDM transfer function from BBKS (*dotted*) and Eisenstein & Hu (*solid*). The results are in good agreement